RESEARCH ARTICLE | MAY 16 2025

On the determinants of electron transfer reorganization energy in a cytochrome P450: cytochrome b5 complex. A combined quantum mechanics and molecular dynamics simulation study

Special Collection: Molecular Dynamics, Methods and Applications 60 Years after Rahman

J. Teuffel ; G. Mukherjee ; S. B. Han ; M. Elstner ; R. C. Wade

J. Chem. Phys. 162, 195101 (2025)
https://doi.org/10.1063/5.0248701

The Journal of Chemical Physics ARTICLE pubs.aip.org/aip/jcp

On the determinants of electron transfer reorganization energy in a cytochrome P450: cytochrome b5 complex. A combined quantum mechanics and molecular dynamics simulation study

Cite as: J. Chem. Phys. 162, 195101 (2025); doi: 10.1063/5.0248701
Submitted: 13 November 2024 • Accepted: 21 April 2025 •
Published Online: 16 May 2025

J. Teuffel,[1,2,3] G. Mukherjee,[1,4] S. B. Han,[1,5] M. Elstner,[6] and R. C. Wade[1,2,4,5,7,a)]

AFFILIATIONS

[1] Molecular and Cellular Modeling Group, Heidelberg Institute for Theoretical Studies, Heidelberg, Germany
[2] Faculty for Engineering Sciences, Heidelberg University, Heidelberg, Germany
[3] Graduate School of Mathematical and Computational Methods for the Sciences (HGS MathComp), Heidelberg University, Heidelberg, Germany
[4] Center for Molecular Biology of Heidelberg University (ZMBH), DKFZ-ZMBH Alliance, Heidelberg University, Heidelberg, Germany
[5] Faculty of Biosciences, Heidelberg University, Heidelberg, Germany
[6] Institute of Physical Chemistry (IPC), Karlsruhe Institute of Technology, Karlsruhe, Germany
[7] Interdisciplinary Center for Scientific Computing (IWR), Heidelberg University, Heidelberg, Germany

Note: This paper is part of the JCP Special Topic on Molecular Dynamics, Methods and Applications 60 Years After Rahman.
[a)]**Author to whom correspondence should be addressed:** rebecca.wade@h-its.org

ABSTRACT

The electron transfer steps in the catalytic cycle of cytochrome P450 (CYP) enzymes, ubiquitous proteins with key roles in processes such as drug metabolism and steroidogenesis, are often rate-limiting. To predict ET rates from atomistic molecular dynamics simulations using Marcus theory, values of the reaction free energy ΔG^0 and the reorganization free energy λ are required from either experiments or computations. For the reduction of cytochrome P450 17A1 (CYP17A1) by the secondary redox protein cytochrome b5 (CYb5), a critical step in the regulation of steroidogenesis, experimental measurements of λ are not available. We here describe the computation of λ for this system from a combination of molecular mechanics/molecular dynamics simulations and quantum mechanics computations. Our results show that a quantum mechanical treatment of the redox-active cofactors is necessary, even though the surrounding protein and solvent, which are modeled classically, contribute most to the reorganization energy. The values of λ computed for structural ensembles corresponding to two predicted binding modes of the proteins are 1.23 and 1.16 eV. We find that the λ values computed for the individual soluble globular domains of the two proteins sum to approximately the λ values computed for the membrane-bound CYP17A1-CYb5 complex, indicating that additivity can be invoked in a computationally efficient approach to estimating λ values for such protein–protein complexes.

I. INTRODUCTION

A. The cytochrome P450 family of monooxidase enzymes and reduction of CYP17A1 by CYb5

A quantitative understanding of electron transfer kinetics is essential for studying cytochrome P450 (CYP) enzymes, as their catalytic mechanism relies on two electron transfer steps. The CYP superfamily encompasses heme (iron-porphyrin)-dependent monooxygenases present in all domains of life that play key roles in biochemical mechanisms, such as steroid hormone biogenesis and drug-metabolism.[1] Their canonical reactive cycle involves the reductive activation of molecular oxygen (O_2) by the iron-porphyrin system and subsequent insertion of one oxygen atom into a hydrocarbon bond (RH) with the second oxygen atom being fully reduced to water,[2]

$$RH + O_2 + 2e^- + 2H^+ \rightarrow ROH + H_2O.$$

Accordingly, the net reaction requires an external supply of electrons from biological redox equivalents like NAD(P)H. Since CYPs (with the exception of CYP fusion proteins) cannot directly bind to and oxidize such molecules, secondary redox proteins form protein–protein complexes with CYPs in which the required electrons are transferred.[3] As a consequence, the ET rates of these processes are relatively slow and, therefore, often rate-limiting.[2]

Mammalian CYPs are membrane-bound and have a transmembrane helix domain (TM-helix) anchoring them to the membrane. This N-terminal TM-helix is connected by a short, flexible linker domain to the catalytic globular domain, which is mostly alpha-helical and surrounds the heme cofactor.[4] Mammalian *type II* CYPs are microsomal, smooth endoplasmic reticulum (ER)-bound enzymes that are particularly important in the metabolism of xenobiotics. They are reduced by their canonical reductase, NADPH-cytochrome P450 oxidoreductase (CPR). In addition, the small heme-protein cytochrome b5 (CYb5) has been shown to be an interaction partner of some CYPs. Its role is not fully understood and varies between CYP isoforms, ranging from reductive to allosteric regulatory.[5] Both CPR and CYb5 have a similar architecture to that of *type II* CYPs with one or more mostly helical domains surrounding their redox-active cofactors and a TM-helix anchoring the proteins to the ER-membrane and a flexible linker domain connecting the two parts.[3,6]

The reduction of these CYPs requires the transient formation of complexes with the membrane-bound redox proteins. Therefore, ET is a complex biophysical process occurring at the interface of an aqueous phase and a lipid phase, dependent mostly on the enthalpically driven association of the soluble, globular domains of the proteins due to the complementary electrostatic potentials of the protein surfaces.[7–11] Many structural and dynamic properties of CYP:redox protein complexes remain elusive. No structure of a membrane-bound CYP:redox protein complex has been solved experimentally at the time of writing this paper, but computational modeling (e.g., in Ref. 12) has been successfully applied to characterize the interactions of CYPs with CPR and other redox proteins.

Cytochrome P450 17A1 (CYP17A1) is a human *type II* CYP that plays a key role in the regulation of steroid hormone biosynthesis. It is of high biochemical and medicinal interest due to its remarkable ability to catalyze both a canonical hydroxylation as well as a subsequent non-canonical lyase activity, enabling the processing of steroid hormone precursor compounds toward different downstream products. While CYP17A1 activity requires reduction by CPR,[13] the non-canonical lyase activity requires co-expression of CYP17A1 with CYb5, providing a biological mechanism for regulating the type of steroid hormones a given tissue produces.[3] The CYP17A1:CYb5 interaction mechanism remains elusive, with some sources suggesting a purely allosteric[14] (i.e., non-reductive) and some a reductive (e.g., Ref. 15) mechanism.

B. Aim and scope

We present a step toward elucidating the mechanism by which CYb5 accelerates the lyase activity of CYP17A1 by computing the reorganization energy λ of binary CYP17A1:CYb5 complexes. λ is a crucial parameter in the calculation of ET rates according to the Marcus theory formalism. In our previous work on modeling such complexes,[12] we used ΔG^0 and λ values derived from experimental measurements to compute ET rates. In the current work, we report the computation of the reorganization energy, λ, for a biphasic (membrane-bound) protein–protein complex comprised of human CYP17A1 and CYb5 in a lipid bilayer, while a detailed biochemical mechanistic investigation of this system will be presented in a separate study.

λ is computed by modeling the educt state of CYP17A1 as the five-coordinated, substrate-bound ferric Fe(III) state and the product state as the ferrous Fe(II) equivalent, i.e., as a five-coordinated, substrate bound ferrous Fe(II) state, similar to a previous study on CYP BM3.[16] Since λ describes the likelihood of sampling the Marcus transition state considering solely the educt and product free energy diabatic surfaces, which are largely determined by the protein and solvent, the computed λ values are applicable even if there are subsequent coupled changes in the heme coordination and surroundings during the catalytic cycle or if electron transfer from CYb5 occurs at another stage of the catalytic cycle.

Furthermore, we aim to elucidate whether a computationally efficient "additive" approach employing computations on the individual proteins only is viable or if the computation of λ has to be performed on the modeled protein–protein complex in a physiological environment to yield accurate results.

II. THEORY

A. Electron transfer processes in biochemical systems

Long-range ET plays a critical role in a variety of biological processes, such as the respiratory chain, photosynthesis, and drug-metabolism (see, e.g., Ref. 17 for a number of biological examples). Electrons are transferred between redox-active cofactors (often transition metal complexes) over distances[18] of 4–24 Å. ET is commonly described according to the semi-classical Marcus theory model.[19,20] Here, the free-energy surfaces of the reactant and product states are modeled harmonically as two diabatic states along a reaction coordinate ["ET reaction coordinate" in Fig. 1(a)]. It has been found that the potential energy difference between the two redox states, termed the ET energy ΔE, representing the collective orientation and redox-state stabilization of the environment, serves as a good reaction coordinate for the description of ET reactions in explicitly solvated systems[21,22] (see Fig. 1).

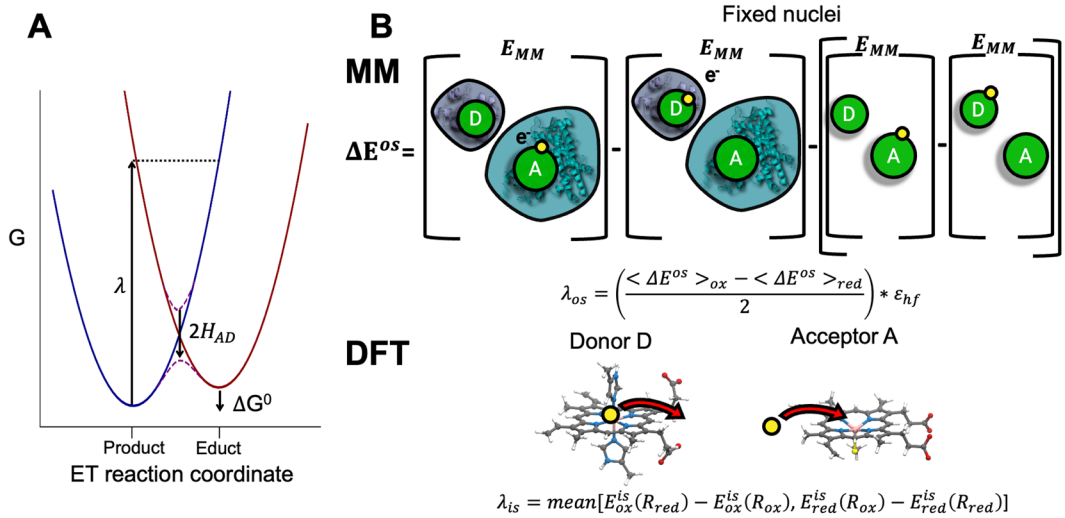

FIG. 1. Models for computing reorganization energies λ for ET reactions. (a) Free energy curves for an ET reaction according to Marcus theory (red: educt/oxidized curve, blue: product/reduced curve). The diabatic product- and educt free energy curves are modeled harmonically along the electron transfer reaction coordinate. Electronic tunneling is characterized by the electronic coupling matrix element H_{AD}, which lowers the activation energy (displayed as purple splines).Note that the figure is not drawn to scale; H_{DA} approaches 0 in the non-adiabatic ET-processes investigated here which are more closely represented by the diabatic surfaces (solid lines). (b) Schematic of the "QM+MM" scheme of Blumberger[25] (with a modification for the computation of ΔE^{os}, see Sec. III A). The problem is split into an MM-based computation of λ_{os} and a DFT-based computation of λ_{is}, where the total reorganization energy λ is the sum of λ_{os} and λ_{is}. λ_{is} of a cofactor is computed from its ground-state geometries in the oxidized and reduced states as the average of the energy gaps at both geometry-minima (see the supplementary material, Fig. S5). For λ_{os}, two structural ensembles, one according to an educt (ox) and one to a product (red) charge distribution, are generated by MD simulation. Then, the classical ET energies ΔE^{os+is} are evaluated for the two trajectories by subtracting the force-field energy according to the "ox" parameterization for a given set of coordinates from the force field energy according to the "red" parameterization for the same coordinates. This yields two distributions of ΔE^{os+is} in the two ensembles. We subtract the classical ET energy of the *inner sphere* computed in the same way for the isolated cofactors from ΔE^{os+is} to yield the classical ET energy of the *outer sphere*: ΔE^{os}. λ_{os} is then computed as half the difference between the expectation values of ΔE^{os} in the product and educt ensembles and scaled by ε_{hf}, which implicitly accounts for the electronic polarizability of the system.

According to the Marcus theory model, two experimentally observable free energies, the reaction free energy, $\Delta G^{0,}$ and the reorganization (free) energy λ, suffice for an analytical description of the free-energy surfaces and all derived properties (here, we use ΔG rather than ΔA, as in some of the ET literature, as we performed simulations in the NP(A)T ensemble). ΔG^0 describes the free energy difference between the well-bottoms of the two surfaces while the λ values are the vertical energy gaps at the two minima: λ_{educt} and $\lambda_{product}$ (see Fig. 1 for a depiction of λ). In the linear response approximation, λ_{educt} and $\lambda_{product}$ are equivalent, yielding a total reorganization energy λ, which defines the curvature of the diabatic free energy surfaces[17] with a harmonic force-constant $k = 1/(2\lambda)$.

As such, the reaction rate k_{ET} can be derived from an analytic expression modeling the free energy difference between the transition state [as the intersection point between the two parabolas from ΔG^0 and λ; see Eq. (1)] and the reactant well minimum where the pre-factor is expressed as a function of the electronic coupling matrix element H_{AD} based on Fermi's golden rule (assuming classical motion of the nuclei),[19,23,24]

$$k_{ET} = \frac{4\pi^2|H_{AD}|^2}{h\sqrt{4\pi\lambda k_B T}} exp\left[-\frac{(\Delta G^0 + \lambda)^2}{4\lambda k_B T}\right], \quad (1)$$

where h is Planck's constant, k_B is Boltzmann's constant, and T is the temperature. The diabatic free energy surfaces and all variables in the above-mentioned equation are depicted in Fig. 1(a).

B. An approach to compute Marcus theory parameters for protein systems from combined quantum mechanics and molecular mechanics simulations

To compute the ET rate in a given system according to Marcus theory, all system-specific parameters, H_{AD}, λ, and ΔG^0 are required to be known. ΔG^0 can be calculated from electrochemically determined redox-potentials. While also a measurable property, accurate estimates of λ are much harder to determine experimentally. The matrix element H_{AD} requires knowledge of the (electronic) structure of the system, is almost impossible to derive with high accuracy for biological systems, and is commonly approximated (see Ref. 17 for an overview of different methods to approximate electronic coupling).

For sufficiently small organic and inorganic molecules, all system-specific ET parameters can be computed from individual (if necessary, Boltzmann-weighted) geometries in quantum chemical computations in the micro-canonical ensemble. However, this approach is not feasible for macromolecules such as proteins in aqueous solution, which adopt a wide ensemble of varied configurations along hundreds to thousands of degrees of freedom. Such systems usually require expensive numerical simulations (e.g., molecular dynamics using molecular mechanics potentials), which often have to be biased to sample processes of interest, and sophisticated analysis protocols are needed to yield meaningful free energies

from such simulations. This is particularly challenging for quantum processes like ET in such systems.

For H_{AD}, empirical schemes to estimate this quantity from structural ensembles of proteins exist, such as the "Dutton"[26] and "Pathways"[27,28] models. These compute H_{AD} as a function of distance between redox-cofactors and, in the latter case, an approximation of the electronic and nucleic structures between them.

To compute λ and ΔG^0 for protein systems, Blumberger proposed a protocol based on decomposing λ (and ΔG^0, which will not be considered in this paper) into *inner sphere: is* and *outer sphere: os* contributions,[25,29]

$$\lambda = \lambda_{is} + \lambda_{os}. \tag{2}$$

λ_{is} accounts for quantum effects on the redox-cofactors themselves and is computed for a region sufficiently small for quantum chemical computations. λ_{os} is instead computed from more efficient classical force field potentials (MM). The system is sampled either in coupled QM/MM or decoupled "QM+MM" calculations, where λ_{os} is computed from a structural ensemble while the significantly smaller and less structure-dependent λ_{is} is evaluated from single-point QM computations [schematically displayed by the separate levels "MM" vs "DFT" in Fig. 1(b)]. As the "QM+MM" approach has been demonstrated to yield acceptably accurate results at a lower computational cost than QM/MM,[25] it is followed in this work.

The protocol for evaluating λ_{os} is based on evaluating the classical potential ET/vertical gap energy ΔE^{os}, which is computed as the difference in force-field energy of a conformation $\mathbf{R}^N$ in the educt and product potentials E_{ox} and E_{red}.[30] The terms "oxidized" and "reduced" are used in the entire paper to distinguish between the educt and product states following the redox-state of the acceptor protein. Here, we subtract the difference in force field energies of the *inner sphere* atoms E^{is} (yielding the ET-energy ΔE^{is}) with the coordinate subset $\mathbf{R}_{is} \in \mathbf{R}^N$ from the total difference in force field energies E^{is+os} to yield ΔE^{os},

$$\Delta E^{os}(\mathbf{R}^N) = E^{os+is}_{red}(\mathbf{R}^N) - E^{os+is}_{ox}(\mathbf{R}^N) - (E^{is}_{red}(\mathbf{R}_{is}) - E^{is}_{ox}(\mathbf{R}_{is})). \tag{3}$$

The "MM" panel in Fig. 1(b) provides a visual depiction of the computation of ΔE^{os} for a single conformation by taking the differences in force field energies for both redox states and subtracting the force-field energies of the inner sphere atoms. Two distributions of ΔE^{os} are computed from MD-based sampling of both potentials in two separate trajectories (named "oxidized" and "reduced" trajectories to indicate which force-field energies were used to compute forces). ΔE^{os} is evaluated over both trajectories, giving two expectation values, $\langle \Delta E^{os} \rangle_{ox}$ and $\langle \Delta E^{os} \rangle_{red}$. Assuming linear response, λ_{os} can be computed from these distributions assuming they are Gaussian and applying a theoretically justified scaling-factor $\varepsilon_{high\,frequency:\ 'hf'} = (1.6)^{-1}$ that implicitly accounts for electronic polarizability (as the inverse of the optical dielectric constants of the medium after some empirical correction),[17]

$$\lambda_{os} = \frac{\langle \Delta E^{os} \rangle_{ox} - \langle \Delta E^{os} \rangle_{red}}{2} * \varepsilon_{hf}. \tag{4}$$

λ_{is} is computed from a simplified "four-point" model (schematically depicted in the supplementary material, Fig. S5) computing the ionization energies at the two respective minimum geometries $\mathbf{R}_{red}$ and $\mathbf{R}_{ox}$, assuming additivity of the two redox cofactors' individual reorganization free energies λ^{Donor} and $\lambda^{Acceptor}$[25]

$$\lambda_{is} = \lambda^{Donor} + \lambda^{Acceptor}, \tag{5}$$

$$\begin{aligned}\lambda^{Donor} &= 1/2((E^{Donor}_{red}(\mathbf{R}_{ox}) - E^{Donor}_{red}(\mathbf{R}_{red})) \\ &\quad + (E^{Donor}_{ox}(\mathbf{R}_{red}) - E^{Donor}_{ox}(\mathbf{R}_{ox})) \\ &= mean(E^{is}_{ox}(\mathbf{R}_{red}) - E^{is}_{ox}(\mathbf{R}_{ox}), E^{is}_{red}(\mathbf{R}_{ox}) - E^{is}_{red}(\mathbf{R}_{red})),\end{aligned} \tag{6}$$

and similarly for $\lambda^{Acceptor}$.

This procedure is displayed in the "DFT" panel of Fig. 1(b), where λ_{is} is computed as the mean of λ_{ox} and λ_{red} from single-point energies on the ground state geometries. We also computed the pure classical reorganization energy λ_{MM}, for which both the *inner* and *outer spheres* are described on a force field level, yielding the total ET energies ΔE^{os+is} (analogous to the first line of Eq. (3) but without subtracting ΔE^{is}). From it, λ_{MM} is computed similarly to λ_{os},

$$\lambda_{MM} = \frac{\langle \Delta E^{os+is} \rangle_{ox} - \langle \Delta E^{os+is} \rangle_{red}}{2} * \varepsilon_{hf}. \tag{7}$$

III. MATERIAL AND METHODS

This section gives an overview of the simulation and parameterization protocols. Additional details on the computation and simulation parameters are given in the supplementary material.

A. Protein structures

The initial structures of binary complexes of substrate (Progesterone/PROG)-bound human CYP17A1 (based on chain C of PDB-ID: 3RUK[31]) and *type A* CYb5 (based on the first model in PDB-ID: 2I96[32]) in two separate binding modes (named CL1 and CL2 (for clusters 1 and 2); see Fig. 2) in a 1-palmitoyl-2-oleoyl-sn-glycero-3-phosphocholine (POPC) phospholipid bilayer were taken from converged simulations (JT, GM, SBH & RCW, unpublished data) in which they were generated following the approach of Mukherjee *et al.*[12] Briefly, two representative encounter complexes of the globular domains were obtained by clustering the rigid-body Brownian dynamics simulation results with SDA 7.3[33–35] of their diffusional association. These complexes were then superimposed on a model of membrane-bound CYP17A1 in complex with progesterone in a POPC lipid bilayer previously obtained by MD simulation,[36] and the transmembrane helices and flexible linker domains were modeled in. The complexes were then simulated in unbiased MD simulations with the CYP cofactor in the *low spin*, water-coordinated ferric state[37] (substrate present but prior to expulsion of the hexagonal water-ligand) and CYb5 in the ferrous state. Subsequently, the final frames of two MD simulations of CL1 and CL2 [simulation-times: 1.63 μs (CL1), 0.77 μs (CL2)] were extracted and re-solvated to be used in this study.

The protonation states were assigned separately for the two systems, resulting in differing net charges of −8 e (CL1) and −9 e (CL2) due to altered degrees of embedding within the POPC lipid bilayer, indicating that further investigation may benefit from constant pH MD simulations.

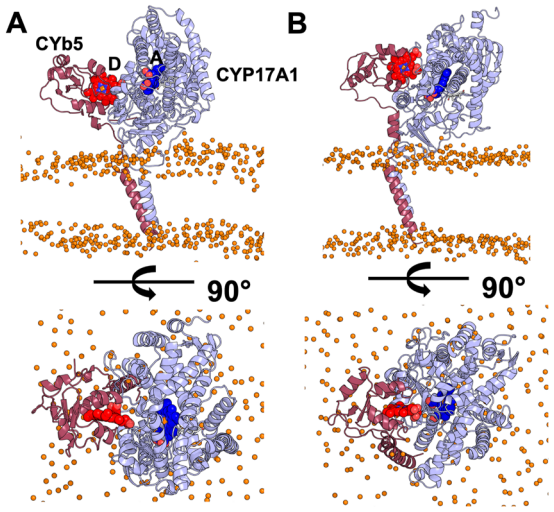

FIG. 2. Two models of binary complexes of CYP17A1 (light blue) and CYb5 (red) in a 1-palmitoyl-2-oleoyl-sn-glycero-3-phosphocholine (POPC) lipid bilayer with two different binding modes that differ slightly in the solvent-exposure of the interface region were used for calculations of reorganization energy (A: CL1, B: CL2) (see text for details). Proteins are displayed in cartoon representation. The electron donor (red carbons) and acceptor (blue carbons) heme-cofactors are displayed as van der Waals spheres. The heme-cofactor in CYb5 donating the electron is labeled "D" (donor), and the heme-cofactor in CYP17A1 is labeled "A" (acceptor). The membrane phosphorus atoms are shown as orange van der Waals spheres. The bound progesterone substrate is displayed in stick representation with gray carbons.

For simulations of the soluble globular domains in aqueous solution, the initial structure of the globular domain of human CYb5 was based on model 1 of an NMR-structure (PDB-ID: 2I96),[32] while the initial structure of the PROG-bound globular domain of CYP17A1 was based on the CL1 input pose. The disordered residues 21 (first resolved residue) to 29 and 111–128 of CYb5 were truncated. For CYP17A1, the membrane-bound residues 1–35, as well as the membrane and CYb5, were removed from the CL1 input structure to yield a soluble, substrate bound structure of the globular domain of CYP17A1.

B. Quantum mechanical computations

DFT calculations for inner-sphere energetics were performed with the ORCA v.5.03 package[38] while RESP charge calculations (and associated geometry optimizations) were performed with the Gaussian09 package.[39] Input geometries were extracted from the respective protein structures.

C. Molecular dynamics simulations

MD simulations were performed using the AMBER14SB force field[40] for the protein and solvent, GAFF[41] for cofactors and ligands for consistency with the heme-parameters of Shahrokh *et al.*,[42] and the Lipid14 force-field[43] for the membranes.

Energy minimizations were performed with AMBER20,[44] and the systems were equilibrated on CPUs using NAMD 2.14.[45] Subsequently, production-run simulations were performed on combined CPU- and GPU nodes with GROMACS 2020.5 (modified RAMD 2.0 release https://github.com/HITS-MCM/gromacs-ramd) for the simulations of the globular domains in aqueous solution or the developer-checked GROMACS 2020.3 release[46] for the simulation of the membrane-bound protein–protein complexes.

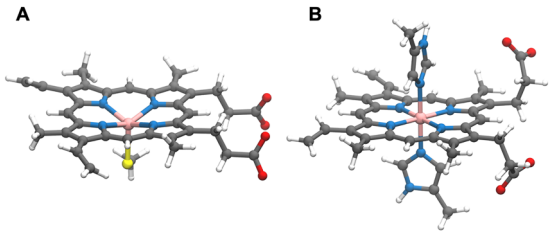

FIG. 3. Iron-porphyrin centers studied at the quantum mechanics level. (a) *High-spin* methylthiolate-heme B from CYP17A1 "MeSHeme" and (b) *low-spin* bi-5-methylimidazole-heme B from CYb5 "MeIm$_2$Heme." Color scheme: carbon: gray, nitrogen: blue, hydrogen: white, oxygen: red, sulfur: yellow, and iron: pale pink.

D. Data analysis

Trajectories were inspected visually with VMD 1.9.3.[47] Radial distribution functions were computed with the "Radial pair distribution" function in VMD 1.9.3,[47] while root-mean square deviations (RMSDs), potential energies, and solvent-accessible surface areas (SASAs) were computed with GROMACS.[46] Subsequent computations were performed with Python (see the supplementary material, Table S4, for a list of all libraries utilized in this study).

E. DFT calculations for *inner sphere* energetics

The cofactors in CYb5 and CYP17A1 were modeled as a *low-spin* hexagonal bi-5-methylimidazole-heme B complex (MeImi$_2$Heme) and a *high-spin* 5-coordinated methylthiolate-heme B complex (MeSHeme) (see Fig. 3). Ground-state geometries were derived at the restricted/unrestricted DFT/B3LYP level of theory using (Zeroth Order Regular Approximation (ZORA)-adapted) relativistic Ahlrich's polarized valence triple zeta basis sets excluding f-polarization from main-group elements. Relativistic effects were incorporated by the scalar relativistic ZORA Hamiltonian.[48] SCF convergence criteria were set to the `TightSCF` keyword, and aqueous solvation was accounted for implicitly with the conductor-like polarizable continuum (CPCM) model.[49] Upon convergence of the geometry optimizations, Hessians were computed analytically or numerically, depending on the system size, to identify saddle-point geometries.

Single-point calculations to compute *inner sphere* reorganization energies were performed in the gas phase using the B3LYP functional using ZORA-def2-TZVP basis sets (including f-type polarization functions) and tight convergence settings. All keyword-lines, relaxed geometries, DFT energies, and spin-contamination values are given in the supplementary material, Table S1. The energies were also evaluated using different exchange-correlation functionals. Blumberger originally proposed the BP and PBE functionals in addition to B3LYP.[25] When testing the other functionals and the range-separated ωB97 functional, we found that all results from these calculations either yielded too low, occasionally negative, values for λ_{is} or suffered from high spin-contamination (see the supplementary material, Table S1).

F. Force-field parameterization of the redox-active cofactors

MM-parameters describing the two different heme-complexes in CYb5 and CYP17A1 were derived independently for this study. In CYb5, the bi-5-methylimidazole heme complex (coordinated by two axial 5-methylimidazole ligands) remains in a *low spin* state in both redox states, with minimal structural changes upon oxidation. This allowed us to use an atom-type-based force-field parameterization, ensuring identical bonded parameters for both redox states.

1. MeSHeme in CYP17A1

The cysteine-heme "residue" in CYP17A1 in its ferric, penta-coordinated redox state was described by parameters from Shahrokh *et al.*[42]

Due to the very small contribution of the inner-sphere region, a simplified approach to the parameterization of the penta-coordinated ferrous cysteine-heme residue was chosen. For this purpose, force-field parameters for the hexa-coordinated ferrous, dioxygen-bound redox-state derived by Shahrokh *et al.*[42] were modified manually, removing the oxygen atoms and redistributing their total partial charge equally over all atoms of the cofactor.

2. bi-5-methylimidazole-heme B in CYb5

The *low spin* bihistidine-coordinated heme in CYb5 was parameterized in this work by deriving restrained electrostatic potential (RESP) charges.

Bonded parameters for the heme and coordinating histidine moieties were assigned from the AMBER18[50] parameter files for histidine and mono-histidine coordinated heme. RESP charges were derived at the HF/6-31G* level using a LANL2DZ effective core potential for the iron atom (the UHF computation for the ferric state required an initial guess from a preceding B3LYP computation). The input geometry had been derived at the B3LYP level with 6-31+G* basis sets for oxygen and nitrogen atoms with constraints on the heme-histidine angle and propionate-histidine distances to avoid intramolecular hydrogen bond formation. Breaking chemical bonds due to the removal of atoms used on the QM-level resulted in residual charges of 0.064 e (ferrous) and 0.3 e (ferric), which were assigned to the heme iron due to its buried location.

All input-lines and force-field parameters for CYb5 are given in the supplementary material.

G. Molecular dynamics simulations of the globular domains of CYb5 and CYP17A1 in aqueous solution

The individual soluble, globular domains of CYP17A1 and CYb5 were immersed in rectangular boxes of TIP3P water molecules and *Na+* and *Cl-*ions at an ionic strength of 150 mM. The two redox states were modeled, and as these differ in the total charge, an additional counter-ion was removed/added to neutralize each system and avoid simulation artifacts.[51]

Protonation states of both proteins were assigned with PROPKA[52,53] (using pdb2pqr 1.9) at pH 7.2.

After energy minimization with AMBER20 (parameters given in the supplementary material, Table S3), the systems were equilibrated in four consecutive steps with NAMD 2.14 in the NPT ensemble using gradually decreasing positional restraints on all heavy atoms of the protein. See the supplementary material, Table S3, for a tabulated description of the energy minimization and equilibration process.

After another unrestrained equilibration in GROMACS in the NPT ensemble, the systems underwent production run simulations of 2 μs each in the NPT ensemble in GROMACS. A Nosé–Hoover thermostat was used (time constant: 1 ps, reference temperature: 310 K), and pressure was controlled with an isotropic Parrinello–Rahman barostat (time constant: 5 ps, reference pressure: 1 bar, compressibility: 4.5×10^{-5} bar^{-1}).The Particle Mesh Ewald method was used to model long-range electrostatics at a Fourier-spacing of 0.12 nm. Bonds to hydrogen atoms were constrained using the LINCS algorithm.

Energies were written every 4 ps for the computation of the classical reorganization energy.

H. Molecular dynamics simulations of membrane-bound CYP17A1:CYb5 complexes

After initial modeling and extended MD-simulation within the resting state (see Sec. III A), the membrane bound CL1 and CL2 assemblies were set up for shorter MD simulations in both reaction states for the reorganization energy computations. For this, the systems were re-solvated using GROMACS. For CL1, the membrane had become too thin in the Y-dimension, which necessitated the generation of new lipids using the "generate symmetry neighbors" function in PyMOL 2.3.[54] To allow the extended membrane to properly equilibrate, an equilibration in NAMD with constraints ("fixed atoms") on all non-solvent, non-lipid atoms was run using otherwise identical parameters to those described in Sec. III G. The final frame of this equilibration was extracted and subjected to production simulations.

The simulation protocol for the binary complexes in the membrane was identical to that for the globular domains in aqueous solution with the following exceptions.

The equilibrations in NAMD were performed in the NPAT (including constant area in x,y) ensemble. All barostats in GROMACS were set to semi-isotropic, and a third temperature-coupling group consisting of the membrane was introduced.

The CL1 systems were each simulated for roughly 320 ns, while the CL2 systems were simulated for 200 ns each.

I. Computation of classical reorganization energies

Classical reorganization energies for all four simulated systems—soluble CYb5, soluble CYP17A1, membrane-bound CL1, and membrane-bound CL2—were computed identically as follows. A visual depiction of the generalized workflow to compute classical reorganization energies is depicted in the supplementary material, Fig. S6.

Force field potential energies (of all atoms, including membrane and solvent) for all analyzed frames of the trajectories were computed with the `gmx energy` program after reevaluating all trajectories with `gmx mdrun -rerun` to yield accurate force-field readouts not subject to LINCS. To compute ΔE^{os+is} according to Eq. (3) (excluding the subtraction of ΔE^{is}), the potential energy of the analyzed coordinates according to the charge distribution in which it has not been simulated is required. This was achieved by generating new topologies based on the respective MM-parameters, and the `gmx mdrun -rerun` feature was used to reevaluate the potential

energy according to this set of force field parameters. The classical reorganization energy of the entire system λ_{MM} was then computed according to Eq. (7).

ΔE^{os} was computed by generating trajectory files of the heme-cofactor and respective ligand(s) only with `gmx trjconv`. Subsequently, `gmx convert-tpr` was utilized to modify the original.tpr files to include only the cofactors, and the trajectories were resampled in both redox states for the atomic coordinates of the cofactors only. From this, the *inner sphere*, MM-based ET energies ΔE^{is}_{MM}, were computed and subtracted from ΔE^{os+is} to yield ΔE^{os}. From this, λ_{os} was computed according to Eq. (4).

Blumberger computed λ_{os} similarly but subtracted the differences between the vertical ionization energies of the two cofactors, not the *inner sphere* ET energy.[25] Our approach additionally incorporates long-range interactions between the cofactors into the *inner sphere* term.

Our "QM+MM" approach requires the breaking of C–C bonds in the amino acid ligands coordinating the cofactors, necessitating the introduction of an additional hydrogen atom in the isolated QM-calculations. The magnitude of any associated error is expected to be small due to the computation of relative energetic quantities and the lack of explicit coupling between the QM- and MM-computations.

The reorganization energy of CYb5 was decomposed into the individual contributions λ^{decomp}_{MM} by generating trajectory-files of the respective sub-systems (e.g., only the protein atoms) including the redox-active heme for the computation of individual ΔEs and subsequent subtraction of ΔE^{is}, yielding a decomposed reorganization energy λ^{decomp}_{MM}.

Uncertainties were estimated as the standard error of the mean: $SEM(\lambda)$ from the SEMs of the ΔE distributions:[55] $SEM(\Delta E^{os/os+is}_{ox/red}) = \mathrm{SD}(\Delta E^{os/os+is})/\sqrt{n}$ (with n being the number of data points and SD being the standard deviation) in Eqs. (4) and (7) according to the propagation of error,

$$SEM(\lambda) = \varepsilon_{hf} * 1/2\sqrt{SEM(\Delta E_{ox})^2 + SEM(\Delta E_{red})^2}. \quad (8)$$

J. Trajectory analyses

Cα RMSDs from the initial structure (after equilibration and prior to production) were computed with the `gmx rms` function for the globular domains only.

Residue-wise solvent-accessible surface areas (SASA) were computed with `gmx sasa`,[56] selecting all non-solvent molecules (excluding lipids) as the solute. The `-or` flag was used to print residue-wise SASAs, and the final 100 ns of each simulation were analyzed.

IV. RESULTS AND DISCUSSION

A. The reorganization energy of the soluble globular domain of CYb5 is influenced by interactions between the redox active heme and mobile cations, analogously to the interaction of CYb5 with positively charged acceptor protein surfaces

Two independent simulations of the globular domain of CYb5 in aqueous solution with the oxidized and reduced heme cofactor were each run for 2 μs. No significant rearrangement of the protein occurred, as indicated by the Cα RMSD from the initial structure remaining around 2 Å (see the supplementary material, Fig. S3).

Subsequently, the MM-ET energies ΔE^{os+is} along the trajectories were evaluated, yielding the two distributions depicted in Fig. 4. From this, a purely MM-based estimation of λ_{MM} was computed (see Table I). The resulting value of 0.5398 eV is slightly higher than the experimentally determined value of 0.44 eV obtained from direct voltammetric measurements on 1-mercapto-1-undecanol-modified Au-electrodes at 0 °C by Blankman *et al.*,[57] but much closer than Dixit *et al.*'s computational estimate of 0.953 eV for *type B* CYb5,[58] who argued that limited flexibility of the protein on the surface of the

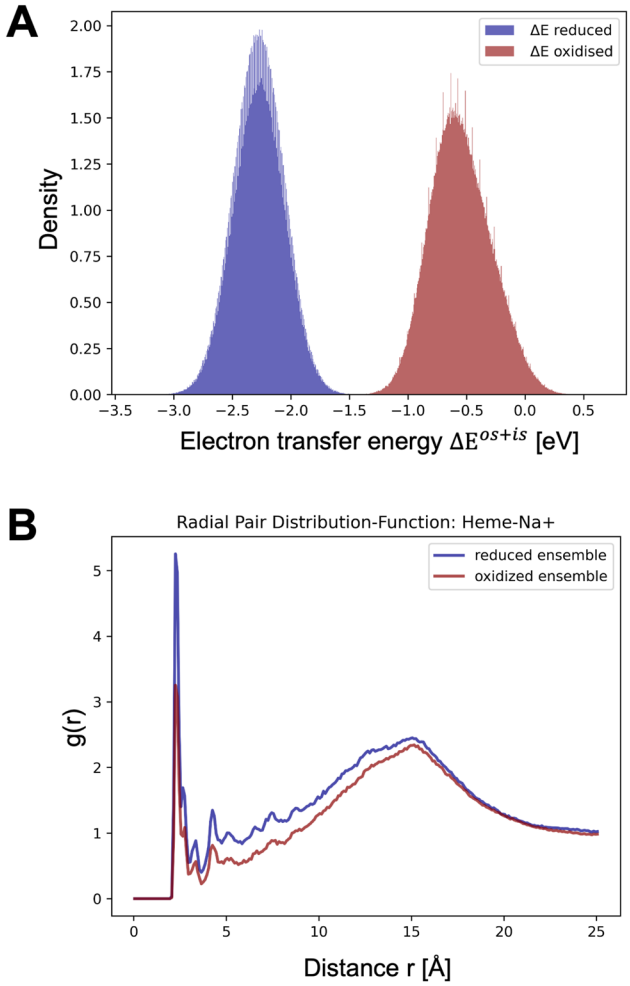

FIG. 4. Computation of the force field reorganization energy λ_{MM} of CYb5. (a) Classical/force field vertical energy gap/ET energy (ΔE^{os+is}) for the oxidized (red) and reduced (blue) trajectories. (b) Sodium-heme radial pair distribution function for the oxidized and reduced ensembles of the CYb5A globular domain, defined as the pairwise distance between sodium cations and any non-hydrogen atom in the redox active heme. The position of the first peak at roughly 2.5 Å corresponds to ion-coordination by the two negatively charged propionate moieties of the heme group. The higher positive charge in the oxidized state increases electrostatic repulsion, weakening the interaction between the propionates on the heme and the cations.

TABLE I. Computed reorganization energies of all studied systems. λ_{MM} refers to values obtained by treating the entire system classically. λ_{os} refers to classical values after subtracting the electron transfer energy of the *inner sphere* atoms. $\lambda_{os} + \lambda_{is}$ refers to λ_{os} summed up with the quantum mechanically computed λ_{is}. The systems "CYb5+CYP17A1" and "CYb5+CYB5" are estimates assuming additivity of the individual proteins' soluble domains' reorganization energies.

System	$\lambda_{MM} \pm \mathrm{SEM}(\lambda_{MM})$ (eV)	$\lambda_{os} \pm \mathrm{SEM}(\lambda_{os})$ (eV)	$\lambda_{os} + \lambda_{is}$(eV)
CYb5	0.5389 ± 0.0001	0.5081 ± 0.0003	0.5714
CYP17A1	2.1711 ± 0.0002	0.6028 ± 0.0011	0.7349
CYP17A1:CYb5 CL1	2.5439 ± 0.0006	1.0371 ± 0.0029	1.2325
CYP17A1:CYb5 CL2	1.9300 ± 0.0010	0.9605 ± 0.0017	1.1559
CYb5+CYP17A1	2.7100	1.1109	1.3063
CYb5+CYb5	1.0778	1.0162	1.1428

electrode could explain the higher value of λ from simulations. It is noteworthy that, while the computational protocols used are similar, our simulations differed in being performed at a higher temperature of 310 K, an ionic strength of 0.15M NaCl, and with a varying number of counter-ions.

The corresponding, more accurate value of $\lambda = \lambda_{os} + \lambda_{is}$ (including the DFT-computations outlined in Sec. IV C) yielded a very similar yet slightly higher value of 0.5714, indicating that the improved accuracy provided by the "QM+MM" protocol makes little difference for CYb5. We conclude that it is possible to compute a sufficiently accurate estimate of λ for a single protein from its two redox states by accounting for its change in partial charge distribution on the cofactor and accompanying this by removal/addition of a positively charged counter-ion. The error introduced by violating the ensemble by varying N is apparently small in contrast to the expected artifacts in MD simulations at non-zero net-charge using PME, which have been found to lead to incorrect counter-ion distributions.[51] Due to the high contribution of the solvent to the computed estimates of λ[59] and the role of counter-ions highlighted in the next paragraph, we decided that MD simulation at neutral charge yet different numbers of particles is preferable for the μs sampling performed.

To investigate the molecular determinants of $\langle \Delta E^{os+is} \rangle$ in this system, we computed the pairwise radial distribution function $g(r)$ of any heavy atom in the heme cofactor with respect to any Na^+ ion for both systems. As depicted in Fig. 4, the value of $g(r)$ is much lower at the close-distance peaks in the oxidized ensemble, particularly around the peak at roughly 2 Å representing direct coordination by the heme-propionate moieties. As the total number of ions was reduced by 1, a small difference is to be expected, but the effect is much larger. It can be explained by the increased net-charge of the solvent-exposed heme-cofactor in the oxidized system, which leads to stronger electrostatic repulsion of the counterions.

To substantiate this observation, the MM-reorganization energy of CYb5 was decomposed into the individual contributions of all groups of atoms in the system (see Table II). The contribution of sodium cations to the total reorganization energy exceeds that of the protein but is smaller than that of the water molecules, indicating that CYb5's reorganization energy is primarily influenced by the solvent (water and ions together contributing 70.5% of λ_{MM}). Equivalent RDF-plots for Cl^- ions showed no noticeable differences (see the supplementary material, Fig. S4).[60]

TABLE II. Decomposition of the classical reorganization energy of the globular domain of CYb5: λ_{MM}^{CYb5} into individual contributions λ_{MM}^{decomp}.

Contributor	$\lambda_{MM}^{decomp} \pm \mathrm{SEM}\,(\lambda_{MM}^{decomp})$ (eV)	$\lambda_{MM}^{decomp}/\lambda_{MM}^{CYb5}$ (%)
Protein	0.1282 ± 0.0003	23.8
Water	0.2034 ± 0.0005	37.7
Cl^-	0.0109 ± 0.0002	2.0
Na^+	0.1655 ± 0.0005	30.7
$MeImi_2$ heme	0.0308 ± 0.0002	5.7

The interaction between CYb5 and CYP17A1 is driven by electrostatic interactions between the negatively charged surface of CYb5 (including the heme-propionates) and cationic residues on CYP17A1. The interaction of mobile cations with the heme is thus analogous to the ionic interactions in the protein–protein complexes. These heme-cation interactions have a remarkable impact on the reorganization energy, contributing almost a third.

B. Differing bonded parameters for the two redox-states of CYP17A1 in the MM-only treatment result in overestimated λ values

For the CYP17A1 globular domain in aqueous solution, the distributions of ΔE^{os+is} differ significantly in their variance, indicating that linear response is not valid. The resulting "MM-only" value for λ_{MM} is also unreasonably high at 2.1711 eV [see Fig. 5(a) for the ET energy distributions].

However, it was found that this effect lies mostly in the *inner sphere* region, as computing ΔE^{os} yields skew but roughly similar distributions with an *outer sphere* reorganization energy λ^{os} of 0.6028 eV [see Fig. 5(b)]. It is likely that this is a consequence of utilizing different bonded parameters in the two simulations, violating linear response, and leading to overestimation of the bonded force-field terms during the resampling procedure. The differences in ground-state geometry between the two sets of bonded parameters mostly concern the heme plane-Fe-S orientation.

The non-Gaussian shapes of the distributions are due to the shape of the subtracted distribution of the MM (force-field) ΔE^{is} depicted in the supplementary material, Fig. S7. The high impact of

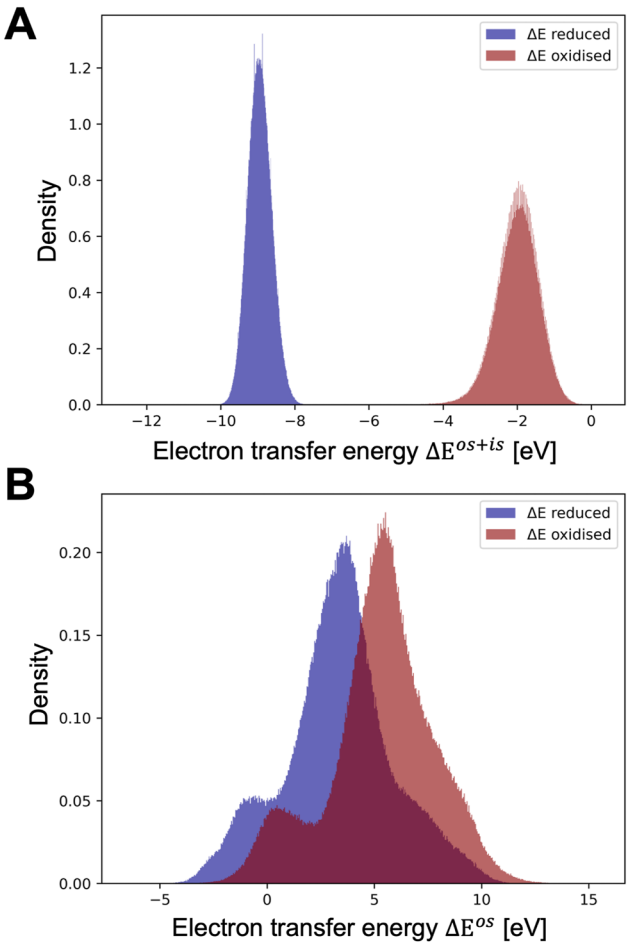

FIG. 5. Classical/force field ET energy/vertical energy gap distributions for the CYP17A1 globular domain in aqueous solution with (a) and without (b) the MM-energies of the heme-cofactor. The strong overestimation of λ_{MM} computed from half the distance between the means and the invalidity of the linear response approximation are a consequence of the different bonded parameters for the two redox states of the redox-active CYP17A1 heme. Subtracting negative distributions of ΔE^{is} with non-Gaussian components (shown in the supplementary material, Fig. S7) shifts the distributions to strongly positive values and results in additional peaks in the tail regions. See the text for further details.

bonded energies on ΔE^{is} renders it more sensitive to small changes in conformation, yielding non-Gaussian artifacts upon small structural fluctuations. Since the non-Gaussian behavior affects mostly the off-center regions of the distributions, additional values of λ^{os} were computed from the peak-positions of the distributions by fitting Gaussian functions; however, this resulted in very small differences compared to taking the mean (see the supplementary material, Table S2). This approach can be interpreted as computing the reorganization energy only for the region of the reaction coordinate obeying the linear response approximation and Marcus theory while inferring that the tail regions are not as important for the electron transfer process. The final "QM+MM" estimate of λ from adding λ_{is} from DFT computations is slightly increased to 0.7349 eV.

C. DFT calculations indicate that the reorganization energies of CYP17A1 and CYb5 are determined by the outer sphere region

Inner sphere reorganization energies of two model systems, a methyl-imidazole heme complex ($MeImi_2$ Heme) and a methylthiolate heme complex (MeSHeme) representing the redox cofactors in the two proteins, were computed from DFT-calculations in vacuum, yielding estimates of $\lambda_{is}^{MeIm2Heme}$ = 0.0633 eV and $\lambda_{is}^{MeSHeme}$ = 0.1321 eV.

According to these computations, λ_{is} is roughly 5-fold smaller than λ_{os} for the proteins. This strengthens the notion that in protein systems obeying Marcus theory, the redox process is mostly determined by the environment formed by the solvent and protein.[17]

D. The reorganization energy of the CYP17A1:CYb5 complex is dependent on the solvent exposure of the heme in CYb5

To compute the system-wide reorganization energy of a binary, full-length CYP17A1:CYb5 complex in a POPC phospholipid bilayer, a pair of production run MD simulations was run for binding mode CL1 for 318 ns (educt state: *ox*) and 316 ns (product state: *red*). As it was found that these simulation times were sufficient for obtaining mostly normally distributed values of ΔE^{os} (as seen depicted in Table I, λ_{MM} was also much overestimated for these systems due to reasons outlined in Sec. IV B), a second set of simulations (each 200 ns) was run for the CL2 binding mode. CL1 and CL2 differ mostly in the rotational orientation of CYb5 on the proximal face of CYP17A1, which affects the interaction of the CYb5 heme with CYP17A1. Notably, the two binding modes display different degrees of solvent-accessibility of the cofactor (see Fig. 2 for a depiction of the two binding modes).

The computed estimates of λ_{os} were 1.0371 eV for CL1 and 0.9605 eV for CL2, differing by 0.0765 eV (see Fig. 6 for the electron transfer energy distributions). Adding the *inner sphere* contributions λ_{is} from DFT-calculations yielded the final values of $\lambda_{os} + \lambda_{is}$ of 1.2325 eV (CL1) and 1.1559 eV (CL2). Both values are relatively close to the estimate of 1 eV (including inner-sphere contribution), proposed by Dutton for interprotein ET[61] and an estimate of 1.15 eV for WT cytochrome P450 BM3 by Dixit *et al.*[16]

To identify why the computed reorganization energies show this relatively small but noticeable difference between the two binding modes of otherwise identical proteins, we computed the solvent-accessible surface area of the heme of CYb5 over the final 100 ns of each simulation (see Table III). The heme is partially solvent exposed in the unbound CYb5 (see Sec. IV A), and it directly participates in the binding-interface between the two proteins in both binding modes.

The SASA of the heme differed by 0.7–0.4 nm^2 indicating that the CL2 assembly can more effectively screen the redox cofactor, thus lowering the reorganization energy by stabilizing charge differences through the protein environment. We have also computed the heme-SASA for the simulation of the CYb5 soluble domain in aqueous solution (see Table III), finding it to exceed the values obtained for the protein–protein complexes despite a much lower reorganization energy. The heme SASA can help to explain the differences in reorganization energies between the two binding modes in the protein–protein complexes. However, as outlined in Sec. IV A,

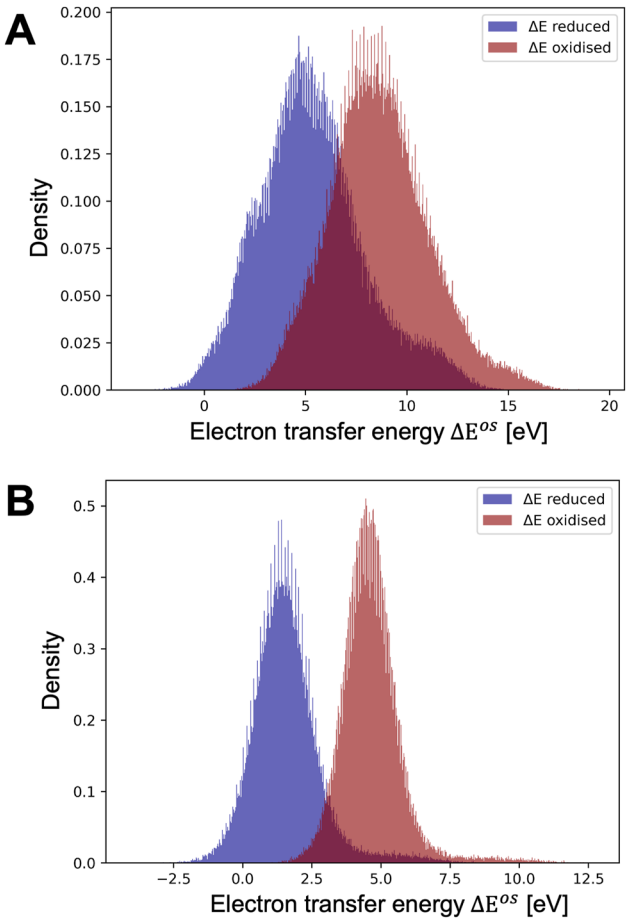

FIG. 6. Classical ΔE^{os} distributions for full-length, membrane-bound binary complexes of CYb5 and CYP17A1. Two different arrangements of the two proteins, CL1 (a) and CL2 (b), were simulated. Their reorganization energies differ slightly due to the differing solvent-exposure of the redox-active cofactors, as indicated by differing distributions (distributions for ΔE^{os+is} of the total systems (λ_{MM}) are displayed in the supplementary material, Fig. S2). The x axis scale is adjusted to the range of values observed in the ensembles and differs between A and B to enable evaluation of the difference between the positions of the mean.

the heme-sodium ion interactions in solution mimic the interaction of the heme propionates with cationic amino acid residues in CYP17A1, which are not included in the computed SASA, preventing a simple quantitative relation between SASA and lambda. In addition, the more complex charge distributions and lower flexibility of the amino acid residues in the protein binding partner provide more effective shielding than the aqueous solvent.

TABLE III. Solvent accessible surface area of the redox-active heme in CYb5 over the final 100 ns of different simulation systems.

System	SASA heme (CYb5) (nm^2)
$CYb5_{ox}$	2.133 ± 0.185
$CYb5_{red}$	2.194 ± 0.217
$CL1_{ox}$	1.662 ± 0.198
$CL1_{red}$	1.500 ± 0.206
$CL2_{ox}$	0.904 ± 0.210
$CL2_{red}$	1.107 ± 0.279

E. The computed QM+MM reorganization energy of the binary CYP17A1:CYb5 complex is approximately the sum of the values computed for the individual unbound redox-active globular domains

It is of practical interest whether computing λ of a protein–protein complex directly from the individual proteins in solution, assuming additivity of the individual reorganization energies of the contributing proteins (e.g., in Ref. 58), yields accurate estimates besides the simplifications taken due to the enormously reduced computational cost and the knowledge required of the structure of the protein–protein complex in question. Summing up the $\lambda_{os} + \lambda_{is}$ values of CYb5 and CYP17A1 (soluble domains only) gives an estimate of 1.3063 eV (CYb5+CYP17A1 in Table I), which is less than 0.1 eV higher than the $\lambda_{is} + \lambda os$ value computed for the membrane-bound protein–protein complex CL1 of 1.232 eV. Likewise, estimating the reorganization energy of homodimeric CYb5:CYb5 self-exchange from doubling λ_{os} summed up with $2 * \lambda_{is}^{MeIm2Heme}$ as 1.1428 eV (CYb5+CYb5 in Table I) compares well to previous computational measurements from Brownian Dynamics simulations of 1.06 eV[62] and experimental estimates between 0.9 and 1.3 eV.[63] As outlined in Sec. IV D, the heme-SASA of Cyb5 does not reflect this trend as it does not include the interactions of the heme-propionates with positively charged amino acid residues on the surface of CYP17A1. The more-effective shielding provided by such interactions may explain why assuming full additivity overestimates the reorganization energies by 6%–13%.

Therefore, we conclude that for this system, a similar approach to that proposed by Blumberger for the cofactors can be taken, significantly reducing computational costs and resource consumption.

V. CONCLUSION AND OUTLOOK

Here, we have described the computation of the reorganization energy of a protein–protein complex in a membrane. This calculation was made possible by employing the "QM+MM" approach of Blumberger.[25] However, the challenging nature of a membrane-bound protein–protein complex system with more than one binding pose required extensive sampling over hundreds of nanoseconds. We found that the reorganization energy is lowered by increased shielding of the redox active heme in CYb5 from the aqueous solvent by the protein–protein interface. Our computed values agree with previous reports on isolated CYb5 as well as the bacterial fusion protein, cytochrome P450 BM3.

The measured reorganization energies are significant beyond this system, given the broad relevance of cytochrome b5 in ET to many CYPs and other redox processes.[5] Since reorganization energy is a rather global property, we believe our results serve as a reliable reference for future studies on CYP and CYb5 redox reactions.

It remains to be evaluated whether our observation that the individual reorganization energies of the globular domains of the two proteins add up to a similar value to that for the complex implies that a simple additive approach can be used for computing reorganization energies of protein–protein complexes in general.

In addition, we demonstrate how this simplification can include neglecting regions that do not participate in the redox reaction, like linker- and membrane-binding domains and the phospholipid bilayer.

SUPPLEMENTARY MATERIAL

The supplementary material contains complete QM energies and spin-contamination values; λ_{os} from Gaussian fits to the electron transfer energies; energy minimization and equilibration parameters; analysis software packages/libraries; outer sphere electron transfer energy plots for soluble CYb5 and total electron transfer energy plots for CL1 and CL2; Cα RMSDs of protein globular domains over all MD simulations; heme Cl- RDF for the soluble CYb5 simulations; visualization of the "four-point" model utilized in the QM calculations; visualization of the workflow to compute classical reorganization energies; classical inner sphere electron transfer energies plot for CYP17A1; QM-program input lines (keywords); and input geometries for QM calculations in xyz format.

Additional supplementary material files: AMBER-format forcefield parameters for His_2Heme in CYb5 (.lib/.prmtop format).

ACKNOWLEDGMENTS

The authors gratefully acknowledge the support of the Klaus Tschira Foundation (SIMPLAIX project 3) and the provision of computing resources by the state of Baden–Württemberg through bwHPC and the German Research Foundation (DFG) through Grant Nos. INST 35/1597-1 (Helix cluster) and INST 40/575-1 FUGG (JUSTUS2 cluster) and by the High Performance Computing Center, Stuttgart, Germany (HLRS; Project Dynathor). The NAMD software was developed by the Theoretical and Computational Biophysics Group in the Beckman Institute for Advanced Science and Technology at the University of Illinois at Urbana-Champaign. The authors acknowledge Stefan Richter for assistance with the technical aspects of the computations, Maja Gruden and Tomas Kubar for advice on methodological aspects of the computations, and Jochen Blumberger and Riccardo Beccaria for their helpful discussions.

AUTHOR DECLARATIONS

Conflict of Interest

The authors have no conflicts to disclose.

Author Contributions

J. Teuffel: Conceptualization (supporting); Data curation (lead); Formal analysis (lead); Investigation (lead); Methodology (lead); Validation (lead); Visualization (lead); Writing – original draft (lead); Writing – review & editing (equal). **G. Mukherjee**: Investigation (supporting); Methodology (supporting). **S. B. Han**: Investigation (supporting). **M. Elstner**: Methodology (supporting); Supervision (supporting). **R. C. Wade**: Conceptualization (lead); Funding acquisition (lead); Supervision (lead); Writing – review & editing (equal).

DATA AVAILABILITY

The data that support the findings of this study are available from the corresponding author upon reasonable request.

REFERENCES

[1]P. R. Ortiz de Montellano, *Cytochrome P450—Structure, Mechanism, and Biochemistry*, 3rd ed. (Kluwer Academic/Plenum Publishers, NY, 2005) pp. 377–610.
[2]F. P. Guengerich, "Mechanisms of cytochrome P450 substrate oxidation: Minireview," J. Biochem. Mol. Toxicol. **21**, 163–168 (2007).
[3]A. V. Pandey and C. E. Flück, "NADPH P450 oxidoreductase: Structure, function, and pathology of diseases," Pharmacol. Ther. **138**, 229–254 (2013).
[4]P. R. Ortiz de Montellano, *Cytochrome P450—Structure, Mechanism, and Biochemistry*, 3rd ed. (Kluwer Academic/Plenum Publishers, NY, 2005) pp. 87–111.
[5]T. D. Porter, "The roles of cytochrome b_5 in cytochrome P450 reactions," J. Biochem. Mol. Toxicol. **16**, 311–316 (2002).
[6]G. Vergères and L. Waskell, "Cytochrome b_5, its functions, structure and membrane topology," Biochimie **77**, 604–620 (1995).
[7]M. Mahajan, T. Ravula, E. Prade, G. M. Anantharamaiah, and A. Ramamoorthy, "Probing membrane enhanced protein–protein interactions in a minimal redox complex of cytochrome-P450 and P450-reductase," Chem. Commun. **55**, 5777–5780 (2019).
[8]D. F. Estrada, A. L. Skinner, J. S. Laurence, and E. E. Scott, "Human cytochrome P450 17A1 conformational selection: Modulation by ligand and cytochrome b5," J. Biol. Chem. **289**, 14310–14320 (2014).
[9]S. Ahuja, N. Jahr, S.-C. Im, S. Vivekanandan, N. Popovych, S. V. Le Clair, R. Huang, R. Soong, J. Xu, K. Yamamoto, R. P. Nanga, A. Bridges, L. Waskell, and A. Ramamoorthy, "A model of the membrane-bound cytochrome b_5-cytochrome P450 complex from NMR and mutagenesis data," J. Biol. Chem. **288**, 22080–22095 (2013).
[10]C. Kenaan, H. Zhang, E. V. Shea, and P. F. Hollenberg, "Uncovering the role of hydrophobic residues in cytochrome P450−cytochrome P450 reductase interactions," Biochemistry **50**, 3957–3967 (2011).
[11]E. Prade, M. Mahajan, S.-C. Im, M. Zhang, K. A. Gentry, G. M. Anantharamaiah, L. Waskell, and A. Ramamoorthy, "A minimal functional complex of cytochrome P450 and FBD of cytochrome P450 reductase in nanodiscs," Angew. Chem., Int. Ed. **57**, 8458–8462 (2018).
[12]G. Mukherjee, P. P. Nandekar, and R. C. Wade, "An electron transfer competent structural ensemble of membrane-bound cytochrome P450 1A1 and cytochrome P450 oxidoreductase," Commun. Biol. **4**, 55 (2021).
[13]A. Y. H. Lu, K. W. Junk, and M. J. Coon, "Resolution of the cytochrome P-450-containing ω-hydroxylation system of liver microsomes into three components," J. Biol. Chem. **244**, 3714–3721 (1969).
[14]R. J. Auchus, T. C. Lee, and W. L. Miller, "Cytochrome b_5 augments the 17,20-lyase activity of human P450c17 without direct electron transfer," J. Biol. Chem. **273**, 3158–3165 (1998).
[15]R. Duggal, I. G. Denisov, and S. G. Sligar, "Cytochrome b_5 enhances androgen synthesis by rapidly reducing the CYP17A1 oxy-complex in the lyase step," FEBS Lett. **592**, 2282–2288 (2018).
[16]V. A. Dixit, U. S. Murty, P. Bajaj, J. Blumberger, and S. P. de Visser, "Mechanisms of electron transfer rate modulations in cytochrome P450 BM3," J. Phys. Chem. B **126**, 9737–9747 (2022).
[17]J. Blumberger, "Recent advances in the theory and molecular simulation of biological electron transfer reactions," Chem. Rev. **115**, 11191–11238 (2015).
[18]C. C. Moser, J. M. Keske, K. Warncke, R. S. Farid, and P. L. Dutton, "Nature of biological electron transfer," Nature **355**, 796–802 (1992).
[19]R. A. Marcus, "On the theory of oxidation-reduction reactions involving electron transfer. I," J. Chem. Phys. **24**, 966–978 (1956).
[20]R. A. Marcus, "Electrostatic free energy and other properties of states having nonequilibrium polarization. I," J. Chem. Phys. **24**, 979–989 (1956).
[21]L. D. Zusman, "Outer-sphere electron transfer in polar solvents," Chem. Phys. **49**, 295–304 (1980).

[22]A. Warshel, "Dynamics of reactions in polar solvents. Semiclassical trajectory studies of electron-transfer and proton-transfer reactions," The J. Phys. Chem. **86**, 2218–2224 (1982).
[23]D. Devault, "Quantum mechanical tunnelling in biological systems," Q. Rev. Biophys. **13**, 387–564 (1980).
[24]R. A. Marcus and N. Sutin, "Electron transfers in chemistry and biology," Biochim. Biophys. Acta, Bioenerg. **811**, 265–322 (1985).
[25]J. Blumberger, "Free energies for biological electron transfer from qm/mm calculation: Method, application and critical assessment," Phys. Chem. Chem. Phys. **10**, 5651–5667 (2008).
[26]C. C. Moser, S. E. Chobot, C. C. Page, and P. L. Dutton, "Distance metrics for heme protein electron tunneling," Biochim. Biophys. Acta, Bioenerg. **1777**, 1032–1037 (2008), a part of Special Issue: 15th European Bioenergetics Conference 2008.
[27]D. N. Beratan, J. N. Betts, and J. N. Onuchic, "Protein electron transfer rates set by the bridging secondary and tertiary structure," Science **252**, 1285–1288 (1991).
[28]I. A. Balabin, X. Hu, and D. N. Beratan, "Exploring biological electron transfer pathway dynamics with the pathways plugin for VMD," J. Comput. Chem. **33**, 906–910 (2012).
[29]J. Blumberger and M. L. Klein, "Reorganization free energies for long-range electron transfer in a porphyrin-binding four-helix bundle protein," J. Am. Chem. Soc. **128**, 13854–13867 (2006).
[30]Blumberger computed *E* solely from the electrostatic MM-energy; in his work, all bonded terms were identical in both states.[25] Here, bonded parameters were different in the reduced and oxidized states of CYP17A1, and we found that the electrostatic energy of the CYP heme-parameters by Shahrokh *et al.* must be combined with the other parameters to yield meaningful energetics.
[31]N. M. DeVore and E. E. Scott, "Structures of cytochrome P450 17A1 with prostate cancer drugs abiraterone and TOK-001," Nature **482**, 116–119 (2012).
[32]M. Nunez, E. Guittet, D. Pompon, C. van Heijenoort, and G. Truan, "NMR strucutre note: Oxidised microsomal cytochrome b5," J. Biomol NMR **47**, 289–295 (2010).
[33]M. Martinez, N. J. Bruce, J. Romanowska, D. B. Kokh, M. Ozboyaci, X. Yu, M. A. Öztürk, S. Richter, and R. C. Wade, "SDA 7: A modular and parallel implementation of the simulation of diffusional association software," J. Comput. Chem. **36**, 1631–1645 (2015).
[34]R. R. Gabdoulline and R. C. Wade, "Brownian dynamics simulation of protein–protein diffusional encounter," Methods **14**, 329–341 (1998).
[35]R. r. Gabdoulline and R. C. Wade, "Simulation of the diffusional association of barnase and barstar," Biophys. J. **72**, 1917–1929 (1997).
[36]G. Mustafa, P. P. Nandekar, T. J. Camp, N. J. Bruce, M. C. Gregory, S. G. Sligar, and R. C. Wade, "Influence of transmembrane helix mutations on cytochrome P450-membrane interactions and function," Biophys. J. **116**, 419–432 (2019).
[37]D. L. Harris, J.-Y. Park, L. Gruenke, and L. Waskell, "Theoretical study of the ligand–CYP2B4 complexes: Effect of structure on binding free energies and heme spin state," Proteins: Struct., Funct., Bioinf. **55**, 895–914 (2004).
[38]F. Neese, "The orca program system," WIREs Comput. Mol. Sci. **2**, 73–78 (2012).
[39]M. J. Frisch, G. W. Trucks, H. B. Schlegel, G. E. Scuseria, M. A. Robb, J. R. Cheeseman, G. Scalmani, V. Barone, B. Mennucci, G. A. Petersson, H. Nakatsuji, M. Caricato, X. Li, H. P. Hratchian, A. F. Izmaylov, J. Bloino, G. Zheng, J. L. Sonnenberg, M. Hada, M. Ehara, K. Toyota, R. Fukuda, J. Hasegawa, M. Ishida, T. Nakajima, Y. Honda, O. Kitao, H. Nakai, T. Vreven, J. A. Montgomery, Jr., J. E. Peralta, F. Ogliaro, M. Bearpark, J. J. Heyd, E. Brothers, K. N. Kudin, V. N. Staroverov, R. Kobayashi, J. Normand, K. Raghavachari, A. Rendell, J. C. Burant, S. S. Iyengar, J. Tomasi, M. Cossi, N. Rega, J. M. Millam, M. Klene, J. E. Knox, J. B. Cross, V. Bakken, C. Adamo, J. Jaramillo, R. Gomperts, R. E. Stratmann, O. Yazyev, A. J. Austin, R. Cammi, C. Pomelli, J. W. Ochterski, R. L. Martin, K. Morokuma, V. G. Zakrzewski, G. A. Voth, P. Salvador, J. J. Dannenberg, S. Dapprich, A. D. Daniels, Farkas, J. B. Foresman, J. V. Ortiz, J. Cioslowski, and D. J. Fox, *Gaussian 09 Revision E.01*, Gaussian, Inc., Wallingford, CT, 2009.
[40]J. A. Maier, C. Martinez, K. Kasavajhala, L. Wickstrom, K. E. Hauser, and C. Simmerling, "ff14SB: Improving the accuracy of protein side chain and backbone parameters from ff99SB," J. Chem. Theory Comput. **11**, 3696–3713 (2015).
[41]J. Wang, R. M. Wolf, J. W. Caldwell, P. A. Kollman, and D. A. Case, "Development and testing of a general amber force field," J. Comput. Chem. **25**, 1157–1174 (2004).
[42]K. Shahrokh, A. Orendt, G. S. Yost, and T. E. Cheatham, "Quantum mechanically derived AMBER-compatible heme parameters for various states of the cytochrome P450 catalytic cycle," J. Comput. Chem. **433**, 119–133 (2013).
[43]C. J. Dickson, B. D. Madej, Å. A. Skjevik, R. M. Betz, K. Teigen, I. R. Gould, and R. C. Walker, "Lipid14: The amber lipid force field," J. Chem. Theory Comput. **10**, 865–879 (2014).
[44]D. A. Case, K. Belfon, I. Y. Ben-Shalom, S. R. Brozell, D. S. Cerutti, T. E. Cheatham III, V. W. D. Cruzeiro, T. A. Darden, R. E. Duke, G. Giambasu, M. K. Gilson, H. Gohlke, A. W. Goetz, R. Harris, S. Izadi, S. A. Izmailov, K. Kasavajhala, A. Kovalenko, R. Krasny, T. Kurtzman, T. S. Lee, S. LeGrand, P. Li, C. Lin, J. Liu, T. Luchko, R. Luo, V. Man, K. M. Merz, Y. Miao, O. Mikhailovskii, G. Monard, H. Nguyen, A. Onufriev, F. Pan, S. Pantano, R. Qi, D. R. Roe, A. Roitberg, C. Sagui, S. Schott-Verdugo, J. Shen, C. L. Simmerling, N. R. Skrynnikov, J. Smith, J. Swails, R. C. Walker, J. Wang, L. Wilson, R. M. Wolf, X. Wu, Y. Xiong, Y. Xue, D. M. York, and P. A. Kollman, *Amber 2020*, University of California, San Francisco, 2020.
[45]J. C. Phillips, D. J. Hardy, J. D. C. Maia, J. E. Stone, J. V. Ribeiro, R. C. Bernardi, R. Buch, G. Fiorin, J. Hénin, W. Jiang, R. McGreevy, M. C. R. Melo, B. K. Radak, R. D. Skeel, A. Singharoy, Y. Wang, B. Roux, A. Aksimentiev, Z. Luthey-Schulten, L. V. Kalé, K. Schulten, C. Chipot, and E. Tajkhorshid, "Scalable molecular dynamics on CPU and GPU architectures with NAMD," J. Chem. Phys. **153**, 044130 (2020).
[46]M. J. Abraham, T. Murtola, R. Schulz, S. Páll, J. C. Smith, B. Hess, and E. Lindahl, "Gromacs: High performance molecular simulations through multi-level parallelism from laptops to supercomputers," SoftwareX **1-2**, 19–25 (2015).
[47]W. Humphrey, A. Dalke, and K. Schulten, "VMD: Visual molecular dynamics," J. Mol. Graphics **14**, 33–38 (1996).
[48]C. van Wüllen, "Molecular density functional calculations in the regular relativistic approximation: Method, application to coinage metal diatomics, hydrides, fluorides and chlorides, and comparison with first-order relativistic calculations," J. Chem. Phys. **109**, 392–399 (1998).
[49]V. Barone and M. Cossi, "Quantum calculation of molecular energies and energy gradients in solution by a conductor solvent model," J. Phys. Chem. A **102**, 1995–2001 (1998).
[50]D. A. Case, I. Y. Ben-Shalom, S. R. Brozell, D. S. Cerutti, T. E. Cheatham III, V. W. D. Cruzeiro, T. A. Darden, R. E. Duke, D. Ghoreishi, M. K. Gilson, H. Gohlke, A. W. Goetz, D. Greene, R. Harris, N. Homeyer, Y. Huang, S. Izadi, A. Kovalenko, T. Kurtzman, T. S. Lee, S. LeGrand, P. Li, C. Lin, J. Liu, T. Luchko, R. Luo, D. J. Mermelstein, K. M. Merz, Y. Miao, G. Monard, C. Nguyen, H. Nguyen, I. Omelyan, A. Onufriev, F. Pan, R. Qi, D. R. Roe, A. Roitberg, C. Sagui, S. Schott-Verdugo, J. Shen, J. Simmerling, C. L. Smith, R. Salomon-Ferrer, J. Swails, R. C. Walker, J. Wang, H. Wei, R. M. Wolf, X. Wu, L. Xiao, Y. D. York, and P. A. Kollman, Amber 2018, University of California, San Francisco, 2018.
[51]J. S. Hub, B. L. De Groot, H. Grubmüller, and G. Groenhof, "Quantifying artifacts in Ewald simulations of inhomogeneous systems with a net charge," J. Chem. Theory Comput. **10**, 381–390 (2014).
[52]C. R. Søndergaard, M. H. Olsson, M. Rostkowski, and J. H. Jensen, "Improved treatment of ligands and coupling effects in empirical calculation and rationalization of pK_a values," J. Chem. Theory Comput. **7**, 2284–2295 (2011).
[53]M. H. Olsson, C. R. Søndergaard, M. Rostkowski, and J. H. Jensen, "PROPKA3: Consistent treatment of internal and surface residues in empirical pK_a predictions," J. Chem. Theory Comput. **7**, 525–537 (2011).
[54]L. Schrödinger and W. DeLano, PyMOL, available at: http://www.pymol.org/pymol, 2020.
[55]We tentatively estimated the standard error of a single lambda by a bootstrapping procedure, yielding values with an accuracy below 1×10^{-6} eV. Due to unfavorable scaling, this was infeasible for all computed reorganization energies.
[56]F. Eisenhaber, P. Lijnzaad, P. Argos, C. Sander, and M. Scharf, "The double cubic lattice method: Efficient approaches to numerical integration of surface area and volume and to dot surface contouring of molecular assemblies," J. Comput. Chem. **16**, 273–284 (1995).
[57]J. I. Blankman, N. Shahzad, C. J. Miller, and R. D. Guiles, "Direct voltammetric investigation of the electrochemical properties of human hemoglobin: Relevance to physiological redox chemistry," Biochemistry **39**, 14806–14812 (2000).
[58]V. A. Dixit, J. Blumberger, and S. K. Vyas, "Methemoglobin formation in mutant hemoglobin α chains: Electron transfer parameters and rates," Biophys. J. **120**, 3807–3819 (2021).

[59] V. Tipmanee, H. Oberhofer, M. Park, K. S. Kim, and J. Blumberger, "Prediction of reorganization free energies for biological electron transfer: A comparative study of ru-modified cytochromes and a 4-helix bundle protein," J. Am. Chem. Soc. **132**, 17032–17040 (2010).
[60] CYb5's net charge is negative in both redox states. Due to this and strong clustering of negatively charged amino acid residues around the heme-binding site, anions experience electrostatic repulsion by this region, leading to a negligible contribution of the Cl^- ions to the electron transfer and reorganization energies.
[61] Golden rules -calculation of electron transfer rates in proteins, https://www.med.upenn.edu/duttonlab/golden.html, accessed 29 October 2024.
[62] S. M. Andrew, K. A. Thomasson, and S. H. Northrup, "Simulation of electron-transfer self-exchange in cytochromes c and b_5," J. Am. Chem. Soc. **115**, 5516–5521 (1993).
[63] D. W. Dixon, X. Hong, S. E. Woehler, A. G. Mauk, and B. P. Sishta, "Electron-transfer self-exchange kinetics of cytochrome b_5," J. Am. Chem. Soc. **112**, 1082–1088 (1990).